# Human Platelet Factor 4 Monomer–Dimer–Tetramer Equilibria Investigated by $^1$H NMR Spectroscopy†

Kevin H. Mayo* and Mu-Jung Chen

*Department of Chemistry, Temple University, Philadelphia, Pennsylvania 19122*

*Received May 19, 1989; Revised Manuscript Received July 25, 1989*

ABSTRACT: As a function of protein concentration, proton NMR spectra of human platelet factor 4 (PF4) differ. Correlation with low-angle laser light scattering data has allowed identification of concentration-dependent NMR spectral changes to PF4 aggregation, with tetramers being the largest aggregates formed. Well-resolved aromatic ring proton NMR resonances were assigned to Tyr-60, His-I, and His-II in monomer, dimer, and tetramer states. Since Tyr-60 3,5 ring proton resonances are well resolved from state to state, estimation of fractional populations in each state was possible. By varying the PF4 concentration, changes in these populations when plotted according to the Hill equation show a bimolecular mechanism of aggregation which proceeds from monomers to tetramers through a dimer intermediate. Equilibrium constants for dimer association ($K_D$) and tetramer association ($K_T$) have been estimated as a function of pH and ionic strength. At pH 4, where $K_D$ and $K_T$ approach the same value, resonances associated with all three aggregate states are observed. Lowering the pH shifts the equilibrium to the monomer state, while raising the pH shifts the equilibrium to dimer and tetramer states. Analysis of the pH dependence of $K_D$ and $K_T$ suggests that electrostatic interactions, probably arising from Glu/Asp and Lys/Arg side chains, play a role in the binding process. Increasing the solvent ionic strength stabilizes the tetramer state especially at low pH, suggesting that intersubunit, repulsive electrostatic interactions probably between/among cationic side chains (Lys/Arg) attenuate the aggregation process. Information based primarily on histidine p$K_a$ values and photo-CIDNP $^1$H NMR data suggests that Tyr-60 and His-I, but not His-II, are significantly affected by the aggregation process.

Platelet factor 4 (PF4),[1] a secretory peptide from $\alpha$-storage granules, is known to strongly bind heparin and other glycosaminoglycans (Barber et al., 1972; Holt & Niewiarowski, 1985) as well as heparan sulfate on the surface of endothelial cells (Busch et al., 1980) and hepatocytes (Rucinski et al., 1987). PF4 may play an important regulatory role in the neutralization of circulating thrombin by antithrombin III in the vascular bed (Busch & Owen, 1981; Marcum et al., 1984), and it is known to stimulate fibroblast attachment to the substrata (Laterra et al., 1983). Other physiological activities of PF4 include stimulation of histamine release from human basophils (Brindley et al., 1983), chemotactic activity with respect to neutrophils, monocytes (Deuel et al., 1981), and fibroblasts (Senior et al., 1983), potentiation of platelet aggregation (Capitanio et al., 1985), and reversal of the immunosuppressive effect of lymphoma cells (Katz et al., 1986).

Human PF4, molecular weight 7800, has been sequenced and contains 70 amino acid residues of which only 3 are aromatic, i.e., His-23, His-35, and Tyr-60 (Deuel et al., 1977; Hermodson et al., 1977; Walz et al., 1977). The presence of antiparallel $\beta$-sheet structure and two cystine disulfide bridges imposes conformational constraints on PF4 backbone folding (Mayo et al., 1989). PF4 monomers are known to associate in a tetrameric structure at low concentration (50 $\mu$g/mL) under physiological conditions (Barber et al., 1972; Moore et al., 1975). On the basis of X-ray crystallographic data, Cowan et al. (1986) proposed a model for the binding of PF4 to heparin in which the monomer subunits associate in a tetrahedral-like array with heparin wound around the outside of this protein core. An X-ray crystallographic structure of the 14–85-residue fragment of tetramer bovine PF4 (St. Charles et al., 1989) shows the presence of three strands of antiparallel $\beta$-sheet and one $\alpha$-helix (C-terminal) in each monomer subunit. The subunits (A, B, C, and D) are arranged in the tetramer, yielding two types of dimers, i.e., AB(CD) and AC(BD), and the tetramer is stabilized by hydrogen bonds, salt bridges, and hydrophobic interactions. A high degree of sequence homology, including the conformationally constraining cystines, between human and bovine PF4s suggests that their overall three-dimensional structures are similar (St. Charles et al., 1989).

Questions regarding the structural organization and stability of PF4 tetramers in solution are important to an understanding of the mechanism of action of this versatile binding protein. Here, NMR spectroscopic techniques are used to study the mode of association, the relative strength of monomer associations, and the nature of subunit interactions for human PF4 in solution. These results are discussed in terms of the crystal structure for bovine PF4 (St. Charles et al., 1989).

## Materials and Methods

*Isolations of PF4.* Outdated human platelets were obtained from the Red Cross and centrifuged at 10000*g* for 1 h to obtain platelet-poor plasma. This preparation was applied to a he-

† This work was supported by a grant from the American Heart Association, South East Pennsylvania (Philadelphia) Section, and benefited from NMR facilities made available to Temple University through Grant RR-04040 from the National Institutes of Health.

* Address correspondence to this author.

[1] Abbreviations: PF4, platelet factor 4; NMR, nuclear magnetic resonance; NOE, nuclear Overhauser effect; rf, radio frequency; FID, free induction decay; CD, circular dichroism; HPLC, high-performance liquid chromatography; CIDNP, chemically induced dynamic nuclear polarization.

0006-2960/89/0428-9469$01.50/0 © 1989 American Chemical Society

parin–agarose (Sigma) column (bed volume 50 mL); the column was washed with 0.2, 0.5, 1, and 1.5 M NaCl. The fraction eluting at 1.5 M NaCl which yielded most of the PF4 (Rucinski et al., 1979) was then desalted by dialysis (0.2% trifluoroacetic acid). The resulting solution was concentrated by lyophilization and further purified by reversed-phase HPLC to yield pure PF4 which was eluted at 38% acetonitrile from a linear $H_2O$ (0.2% TFA)/acetonitrile (0.2% TFA) gradient. From about 50 units of outdated platelets, 15 mg of HPLC-purified PF4 generally resulted.

*Low-Angle Laser Light Scattering.* Experiments were performed by using a KMX-6 photometer (LDC/Milton Roy, Milton Roy Co., Sunnyvale, CA) equipped with a thermostated flow cell kept at 25 °C for these studies. Purified PF4 was dialyzed at 4 °C against 1 mM NaCl, pH 3 or 4, and was centrifuged at 20000*g* for 1 h immediately before use. The sample was brought to 25 °C and pumped from a syringe through a prewashed 3-mm diameter, 0.20-$\mu$m pore size nylon filter (Micron Separation, Indc., Honeyoye, NY) and then through the flow cell of the photometer at 0.09 mL/min using an infusion pump (Sage Instruments Division, Orion Research Inc., Cambridge, MA). After stable scattering readings had been obtained, the solution emerging from the flow cell was collected to accurately determine protein concentration in the light path. Measurements were made at several protein concentrations, using a 0.3-mm field stop, yielding Rayleigh scatter values of (2.3–21) $\times 10^{-6}$ cm$^{-1}$; the $R_\theta$ of the background salt solution was $2 \times 10^{-6}$ cm$^{-1}$. The data were analyzed by a linear least-squares fit to yield a weight-average molecular weight and were plotted as $K_c/R_\theta$ vs PF4 concentration.

*Protein Concentration.* Protein concentration was determined by the method of Lowry et al. (1951), and results were calculated from a standard dilution curve of human serum albumin. An alternative method used to determine PF4 concentration was that of Waddell (1956).

*Nuclear Magnetic Resonance (NMR) Spectroscopy.* Samples for $^1$H NMR measurements had been lyophilized and redissolved in $^2H_2O$ immediately before the experiment. The final protein concentration ranged from 0.5 to 12 mg/mL as indicated in the text. The p$^2$H was adjusted by adding microliter increments of NaO$^2$H or $^2$HCl to a 0.6-mL sample. All measurements were done at the p$^2$H value indicated in the text read directly from the pH meter and not adjusted for isotope effects.

$^1$H NMR spectra were recorded in the Fourier mode on a GE Omega 500 spectrometer (500 MHz for protons). The solvent deuterium signal was used as a field-frequency lock. All chemical shifts are quoted in parts per million (ppm) downfield from sodium 4,4-dimethyl-4-silapentanesulfonate (DSS).

Two-dimensional NOESY (Jeener et al., 1979) NMR spectra (mixing time of 0.2 s) were accumulated in $^2H_2O$ as 512 time-incremented, 1024-point spectra in the phase-sensitive mode (Marion & Wüthrich, 1984). Data processing was done on a Sun -3/160 computer with software supplied by GE on the spectrometer. FIDs were first multiplied by a Lorentzian–Gaussian transformation or shifted sine-bell function, and data sets were zero-filled to 1024 in the evolution dimension.

*Photo-CIDNP NMR Experiments.* Samples for photo-CIDNP experiments contained about 2 mg/mL PF4 in $^2H_2O$. Flavine dye [3-*N*-(carboxymethyl)lumiflavine, generously provided by Dr. F. Muller, University of Wageningen, Wageningen, The Netherlands] was used at a concentration of 0.4 mM. Photo-CIDNP proton NMR spectra were recorded on a Bruker HX-360 spectrometer controlled by an Aspect 2000 computer. A Spectra Physics Model 171 argon ion laser was employed as the light source. A 0.5-s light pulse (4 W, multiline) was used with a 0.05-s delay before the 90° radio-frequency pulse. The "neat" photo-CIDNP response was induced by irradiating the sample with laser light after two saturation pulse trains of 2 s each. Four "light" scans were accumulated for each spectrum. Although the photo-CIDNP enhancement was quite large, it was necessary nevertheless to subtract four "dark" transients normalized for each "light" scan in order to remove residual background magnetization.

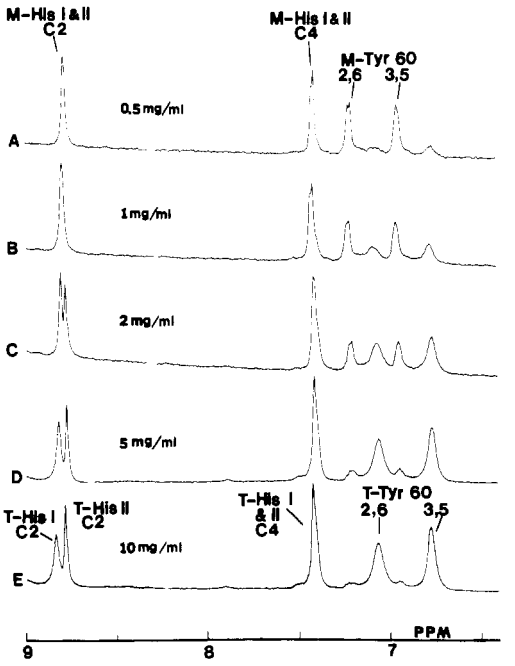


FIGURE 1: Proton NMR spectra of PF4. 500-MHz proton NMR spectra of human PF4 are shown. Lyophilized protein samples were dissolved in $^2H_2O$ at pH 3.0, 303 K, containing PF4 concentrations as listed in the figure. No buffer or salt was added to these solutions. The resonance label prefixes M, D, and T stand for monomer, dimer, and tetramer states, respectively.

## Results

Under the same solvent conditions (i.e., pH, ionic strength, temperature), different concentrations of PF4 give somewhat different proton NMR spectra. Figure 1A shows the aromatic region of a spectrum taken with a relatively low concentration of 0.5 mg/mL, while Figure 1B–E shows spectra taken with increasing concentrations. It is known that PF4 at physiologic pH can aggregate in solution to the tetramer state (Moore et al., 1975) which is a likely explanation for observed spectral changes due only to a variation in protein concentration. Since PF4 contains only three aromatic residues, i.e., His-23, His-35, and Tyr-60, whose ring proton resonances are well resolved, we have focused our attention on these side chain resonances. At the highest PF4 concentration (Figure 1E), the two most intense, upfield resonances have been assigned to the 2,6 and 3,5 ring proton resonances of Tyr-60 in the tetramer state (Mayo et al., 1989). Lowering the protein concentration reduces the intensity of these resonances, while increasing the intensity of two other more downfield resonances at 7.2 and 6.95 ppm. These resonances are less broad and show an apparent, resolved splitting of 8 Hz; moreover, their intensities change in a 1:1 ratio as the concentration is varied. These data are consistent with the idea that they belong to Tyr-60 in a lower aggregate state, most probably monomer as labeled in Figure 1. His-I and His-II (i.e., His-23 and His-35) C2 and

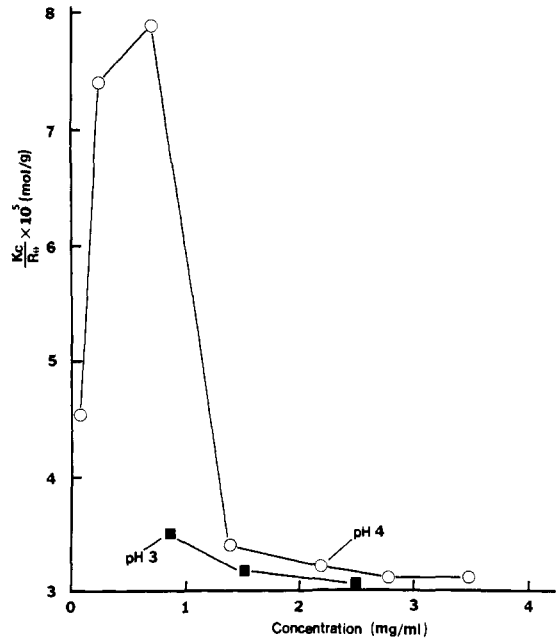


FIGURE 2: Molecular weight determination of PF4 by low-angle laser light scattering. Plot of $K_c/R_\theta$ as a function of PF4 concentration in the scattering cell yields an ordinate intercept indicating the weight-average molecular weight as discussed in the text. Data are shown for pH 3 and 4. Lines connect actual data points only as visual aids.

C4 ring proton resonances likewise show concentration-dependent spectral changes also most probably associated with aggregation state. Other not as well-resolved, more upfield resonances have also been apparently shifted and broadened (data not shown).

Low-angle laser light scattering was used to assess the state of aggregation under the present experimental conditions; earlier sedimentaton equilibrium experiments (Moore et al., 1975) which showed the existence of PF4 tetramers were done at pH 7.4 and at a much lower protein concentration (50 $\mu$g/mL). Higher concentrations of PF4 could give rise to higher aggregation states. The weight-average molecular weight of the PF4 aggregate was obtained from the oridinate intercept of a plot of $K_c/R_\theta$ as a function of PF4 concentration, $c$, as shown in eq 1. The Rayleigh light scattering factor, $R_\theta$,

$$K_c/R_\theta = 1/M + 2A_2c \quad (1)$$

was determined by using a 6–7° annulus. In eq 1, $A_2$ is the second virial coefficient; $R_\theta$ has been corrected by subtracting the effect from the solvent, and $K$ is an optical constant given by

$$K = 2\pi^2n^2(dn/dc)^2(1 + \cos^2\theta)/\lambda^4N \quad (2)$$

in which $\lambda$ is the wavelength of the incident light (632.8 nm), $N$ is Avogadro's number, $\theta$ is the angle at which scattered light is measured, $n$ is the refractive index of the medium, and $dn/dc$ is the differential refractive index increment of the protein which we assumed to be 0.18 mL/g, a value found for most proteins (Perlmann & Longsworth, 1948).

In Figure 2, $K_c/R_\theta$ is plotted versus PF4 concentration for light scattering data acquired at pH 3 and at pH 4. At the highest concentrations, a limiting weight-average molecular weight of 32 500 is estimated. This value shows that the highest state of aggregation is tetramer PF4 and confirms the NMR assignment of aromatic ring proton resonances in the tetramer state. As the protein concentration is lowered from 2.5 mg/mL to about 1 mg/mL, $K_c/R_\theta$ increases slightly, yielding a negative slope of 33.3 mol·mL/g$^2$. This negative

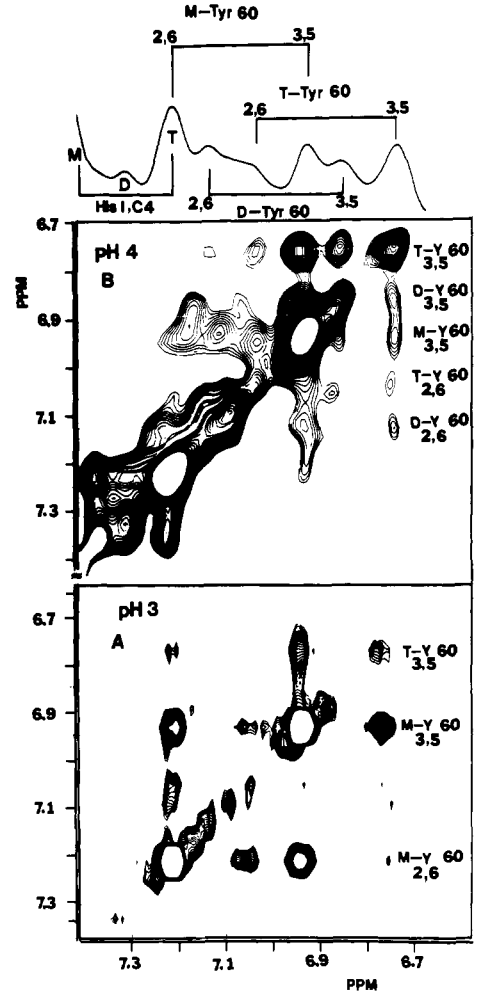


FIGURE 3: NOESY contour plot. The Tyr-60 chemical shift regions of NOESY contour plots of PF4 at pH 3 (A) and pH 4 (B) are shown. At the top of the figure is shown a 1D trace taken from the pH 4 2D data set (5 Hz per point). The mixing time was 0.2 s, and other experimental details are given under Materials and Methods. At pH 3, the data were processed with a Lorentzian to Gaussian transformation in both $t_1$ and $t_2$ time domains prior to Fourier transformation. At pH 4, more broadened line widths required a 90° shifted sine-Bell function multiplication of the raw data.

value, corresponding to the second virial coefficient, reflects the existence of protein aggregation (Tanford, 1961). The reciprocal of the oridinate intercept (extrapolated) yields a weight-average molecular weight of 26 300. When the concentration of PF4 is lowered to below about 1 mg/mL at pH 3 and 0.5 mg/mL at pH 4, where probably mostly monomer PF4 should be present, $R_\theta$ surprisingly increases dramatically, leading, therefore, to a fall in $K_c/R_\theta$. Since it is unlikely that soluble, high molecular weight PF4 aggregates are forming at lower protein concentrations, the most acceptable explanation is the "sticking" of PF4 monomers to the quartz surface of the optical flow cell which holds the sample solution. This effect is easily removed by purging the cell with water. It is unclear why this happens. It only occurs, however, when the protein concentration is below that used in NMR experiments.

Interestingly, at pH 4, but not at pH 3, values for $R_\theta$ can be observed down to 0.1 mg/mL. Below this concentration, $R_\theta$ is too large to measure as mentioned above. At about 0.5 mg/mL, $K_c/R_\theta$ reaches $8 \times 10^{-5}$ mol/g before falling precipitously. If one extrapolates to the ordinate intercept (negative slope of $7.1 \times 10^{-2}$ mol·mL/g$^2$), a weight-average molecular weight of 8300 can be estimated. This estimate corresponds nicely to the molecular weight of monomer PF4.

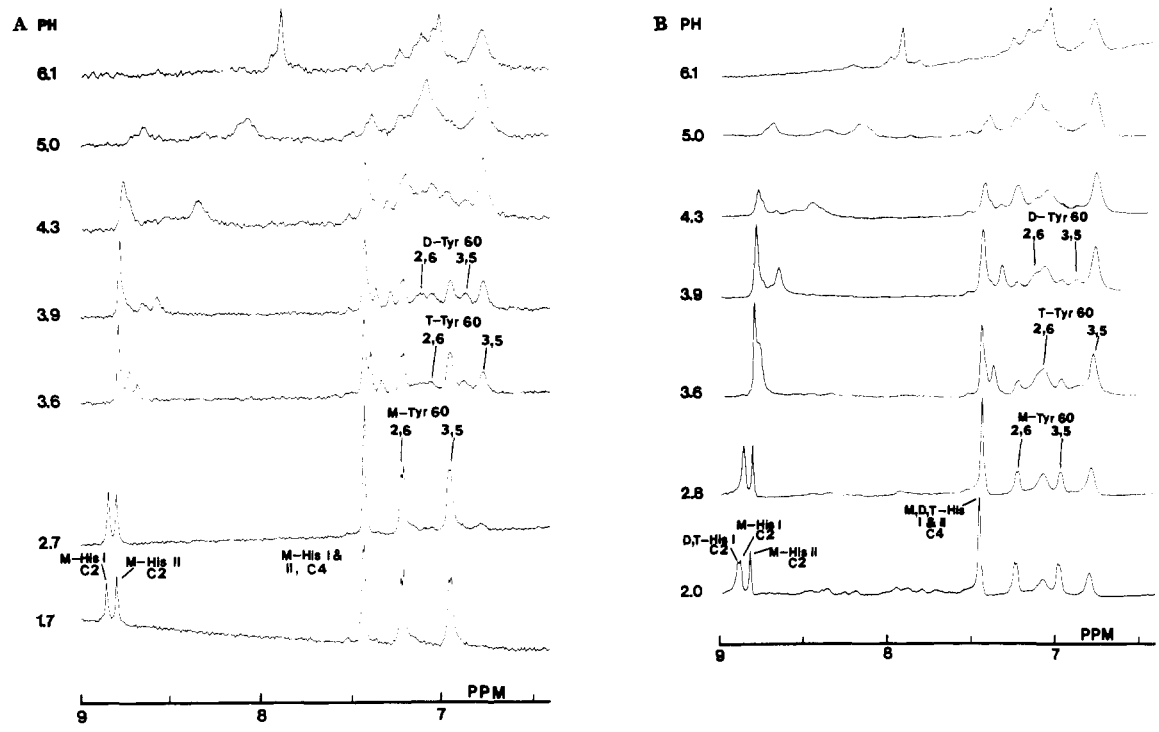


FIGURE 4: Effect of pH and concentration on PF4 aromatic proton resonances. A series of proton NMR spectra taken in $^2H_2O$ are shown for the PF4 aromatic resonance region as a function of solution pH indicated in the figure next to each spectrum. The two panels are for PF4 concentrations of 1 mg/mL (A) and 4 mg/mL (B). The temperature was 303 K. The resonance label prefixes M, D, and T stand for monomer, dimer, and tetramer states, respectively.

A 2D NMR NOESY contour plot of the Tyr-60 spectral region (Figure 3A) shows the expected nuclear Overhauser effect between Tyr-60 2,6 and 3,5 ring proton resonances in monomer PF4 which is present at about 90% in this preparation; tetramer PF4 accounts for the remaining 10%. Unexpected cross-peaks are also present, however, between monomer and tetramer Tyr-60 resonances. This shows that relatively slow exchange on a 500-MHz time scale is occurring between monomer and tetramer PF4. If we raise the pH to 4, a 1D NMR spectrum (top of Figure 3) shows the appearance of new resonances lying between Tyr-60 monomer and tetramer ones, while a NOESY contour plot (Figure 3B) gives cross-peaks between these new resonances and among these and Tyr-60 monomer and tetramer resonances. Since resonances in this 2D data set were broader than normal, spectral phasing was difficult, and cross-peaks appear to have lower intensity on one side of the contour plot diagonal. These new resonances may arise from Tyr-60 2,6 and 3,5 ring proton resonances in a dimer state. Moreover, since Tyr-60 resonances in all three states give NOESY cross-peaks among each other, this demonstrates the existence of exchange among states which is consistent with the presence of monomer–dimer–tetramer equilibria.

*Equilibrium Constants for Aggregation and the Effect of pH.* Figure 4A,B presents representative spectra at two PF4 concentrations as a function of pH. At pH values above about 6, PF4 solubility drops significantly, and data could not be collected. Tyr-60 resonances, in particular, are well resolved and not chemically shifted by pH variations. As the PF4 concentration is increased at a given pH value, the tetramer Tyr-60 resonance population increases as the monomer population decreases. When the pH is around 4, one notices that between tetramer and monomer Tyr-60 resonances, new resonances appear as observed in the NOESY spectrum (Figure 3B) and vary in intensity as a function of PF4 concentration. Since light scattering data show that no aggregates larger than tetramers form with PF4, it is perhaps logical to assume that these new resonances do indeed arise from PF4 dimers. The following analysis is given to demonstrate this to be correct. Since the total area under all Tyr-60 resonances remains constant, one can estimate the mole fraction for each state, and by knowing the total protein concentration in terms of moles of Tyr-60, one can estimate the PF4 concentration in each state. The general equation for association is given by

$$n\mathrm{M} \rightleftharpoons \mathrm{M}_n \qquad (3)$$

where M stands for monomer and $n$ is the stoichiometric coefficient; the symbol $M_n$ stands for the aggregation state. The association equilibrium constant, $K$, expression is given by

$$K = [\mathrm{M}_n]/[\mathrm{M}]^n \qquad (4)$$

and rewriting in terms of natural logarithms, one gets

$$\ln [\mathrm{M}_n] = n \ln [\mathrm{M}] + \ln K$$

where the brackets refer to concentration. If we plot ln $[M_n]$ versus ln [M] at a pH value of 3 (Figure 5) where $M_n$ is identified with the Tyr-60 tetramer resonances and M is taken to be the monomer resonances, we arrive at a value for $n$ of 4.2 which shows that four subunits are associating to yield tetramers as known from light scattering data. This supports the assignment for monomer Tyr-60 resonances. If one now makes similar plots for pH 4 data where the assumed "dimer" resonances are taken as $M_n$ in eq 4 and ln $[M_n]$ is plotted versus ln [M], we derive a slope, $n$, of 1.7. Doing the same but with M standing for "dimer" resonances and $M_n$ for tetramers, we again attain a slope, $n$, of about 2. These data confirm the assignment of Tyr-60 resonances in the dimer state and provide evidence for the normally observed bimolecular mechanism of association going from monomers to dimers and then from dimers to tetramers. This is shown in eq 5 where

$$2\mathrm{M} \rightleftharpoons \mathrm{D} \qquad \text{and} \qquad 2\mathrm{D} \rightleftharpoons \mathrm{T} \qquad (5)$$

M stands for monomer, D for dimer, and T for tetramer. For

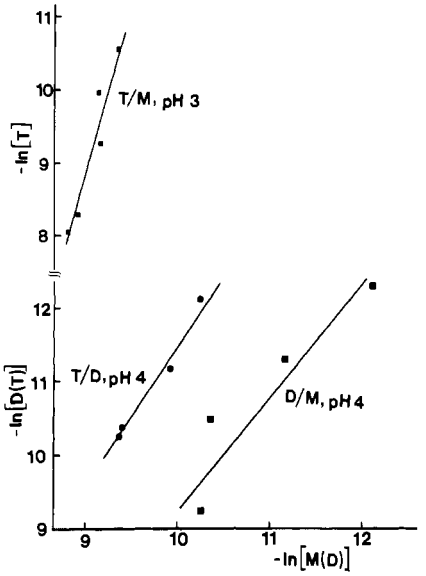


FIGURE 5: Hill plots for dimer and tetramer formation. Fractional populations for monomers (M), dimers (D), and tetramers (T) were extracted from the NMR data as a function of PF4 concentration as described in the text. The natural logarithm of the presumed tetramer (or dimer) concentration was plotted versus that of the dimer (or monomer) concentration to yield a slope which gave the number of associating subunits according to eq 4. The solid lines represent least-squares fits of the data.

these equilibria, equilibrium constants for association are given as

$$K_D = [D]/[M]^2 \quad \text{and} \quad K_T = [T]/[D]^2$$

Having assigned well-resolved, Tyr-60 3,5 ring proton resonances to a specific state of aggregation, we have at hand an easy method to monitor aggregate equilibria and estimate equilibrium constants. Knowing the mole fraction of M, D, and T derived from resonance integrals and the total protein concentration per mole of Tyr-60 allows one to estimate the effect of pH on the association equilibrium constants, $K_D$ and $K_T$, from data like those shown in Figure 4. This effect is shown in Figure 6 for pH values where it was practical to estimate appropriate mole fractions for monomer, dimer, and tetramer. In cases where only monomer and tetramer populations could be estimated, the overall association equilibrium constant, $K_{DT}$, is shown; this is equal to $K_T \times K_D^2$. At about pH 4, $K_T$ is at a minimum, and $K_D$ approaches the value of $K_T$. The main reason that dimer populations can be observed around pH 4 is due, therefore, to more similar values of $K_D$ and $K_T$. As the pH is lowered, $K_T$ increases while $K_D$ falls; by pH 2, the monomer state is highly favored due to the weakened dimer association, and any dimers that do form readily associate to form tetramers by virtue of the relatively larger $K_T$ value. As the pH is raised to values above pH 4, $K_T$ and $K_D$ increase. Above about pH 5, estimates of mole fractions could not be made since Tyr-60 monomer and dimer populations were too small to be accurately measured.

The pH dependence of association could be the result of several factors related to the nature of monomer–monomer and dimer–dimer associatons. Two types of charge interactions could cause association to increase with decreasing pH as is the case with dimer–dimer associations below pH 4: (1) if there were a pair of interacting carboxyls, protonation of one would eliminate the unfavorable (repulsive) electrostatic interaction; (2) protonation of a neutral side chain, with the creation of a positive charge, could result in a favorable interaction with a negatively charged side chain. Decrease in

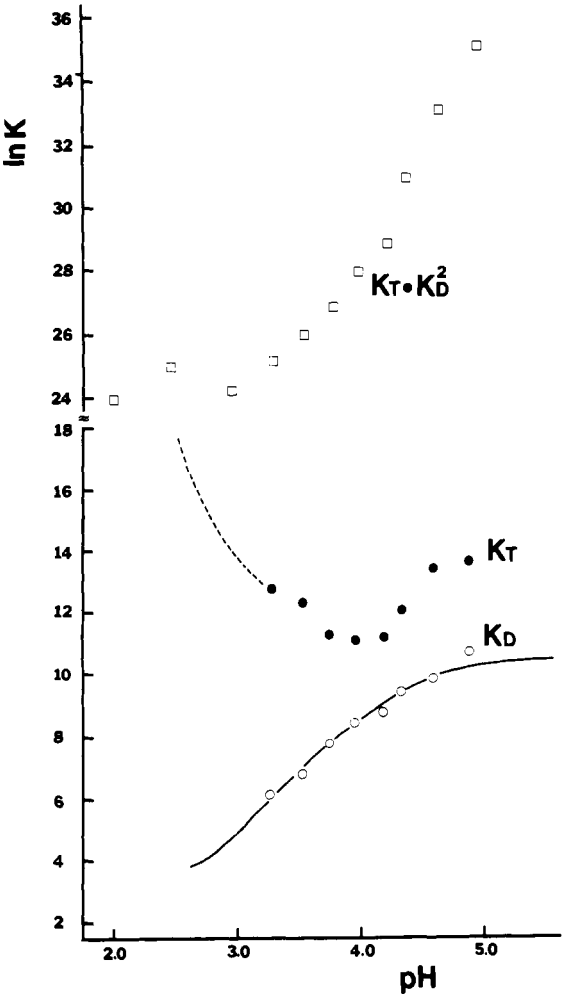


FIGURE 6: Effect of pH on equilibrium constants, $K_i$. Plots are shown for ln $K_T$ and ln $K_D$ versus pH. Values for $K_T$ and $K_D$ were derived as discussed in the text. The overall equilibrium constant, $K_{DT}$ ($=K_T K_D^2$), is also given. The solid line through $K_D$ values represents the best fit of the data to eq 8. The dashed line extending the $K_T$ estimates was calculated from $K_{DT}$ values and the completed function of $K_D$ vs pH.

association with decreasing pH could be accounted for by (1) the elimination of an attractive cationic–anionic interaction by the protonation of the anionic group or (2) the increasing unfavorable long-range electrostatic repulsion between two macroions with a net positive charge. Alternatively, pH-induced conformational transitions could be occurring. The uptake or release of protons by the protein could perhaps allow certain speciic side chains to assume new conformational states which could result in the above types of favorable or unfavorable electrostatic interactions. These new interactions could strengthen or weaken protein associations by either creating or eliminating hydrogen bonds or properly matching hydrophobic sites. It is unlikely, however, that gross conformational changes are occurring under the conditions studied for several reasons: (1) we are dealing with a narrow pH range; (2) two disulfide bridges which impose structural constraints on PF4 are not modified by these pH changes; and (3) below pH 4, tetramer association is enhanced while dimer association is attenuated, suggesting that protein denaturation at least down to pH 2 is not occurring.

Assuming that conformational changes, if they do occur, are minimal, the pH dependence of association can be analyzed to a first approximation in terms of interactions between ionizable groups fixed in space. This type of analysis was used for the study of $\alpha$-chymotrypsin dimerization (Aune et al.,

1971) and is based on the ligand activity relationships developed by Wyman (1964), who showed that

$$\left(\frac{\partial \ln K}{\partial \ln a_i}\right)_{a_{j\neq i}} = \Delta\nu_l \quad (6)$$

where $K$ is the apparent equilibrium constant, $a_l$ is the activity of the ligand which perturbs the equilibrium, i.e., $H^+$ in this case, and $\Delta\nu_l$ is the difference between the numbers of bound ligand molecules to the two states in equilibrium. For our case, the equation becomes

$$\Delta\nu_H = \nu_H^{D(\text{or T})} - 2\nu_H^{M(\text{or D})} \quad (7)$$

where the superscripts M, D, and T represent monomer, dimer, and tetramer, respectively. The maximum absolute value of $\Delta\nu_H$ deduced from the slope in Figure 6 is between 3.5 and 4 for both dimer and tetramer association. The simplest explanation is to assume that four groups are involved in each level of interaction. This value is plausible since 2-fold symmetry axes are suggested to exist between dimer pairs by comparison to tetramer bovine PF4 (St. Charles et al., 1989). This would mean that an interacting charge group on one monomer subunit is symmetry related to the same group on an opposing monomer subunit. In other words, we are probably dealing only with two different side chains in monomer–monomer (dimer) interactions and another two side chains in dimer–dimer (tetramer) interactions.

The pH dependence of the association (dimerization) equilibrium constant is given by

$$\ln K = \ln K(\text{pH} = \infty) + 2\ln\left[\frac{(1 + a_H/K_{1,D})(1 + a_H/K_{2,D})}{(1 + a_H/K_{1,M})(1 + a_H/K_{2,M})}\right] \quad (8)$$

where $a_H$ is essentially given by the hydrogen ion concentration and $K_1$ and $K_2$ are the ionization constants for the interacting groups in M and D states, respectively (or D and T states, respectively, as the case may be). The data of Figure 6 were iteratively curve fitted to this expression. Only in the case of monomer–monomer (dimer) association was a satisfactory fit attained as shown by the solid line in Figure 6. This yielded values of $pK_{1,M} = 4.0$ and $pK_{2,M} = 8.7$; on dimerization, the values changed to $pK_{1,D} = 2.3$ and $pK_{2,D} = 10.3$. The $pK_a$ values of these interacting groups are most readily identified with Glu/Asp and Lys/Arg side chain ionizations.

The eq 8 fit for monomer–monomer association data shown in Figure 6 indicated that $K_D$ should plateau out at about pH 5 and reach a minimum at about pH 2.5. Since we have estimates for $K_{DT}$ ($=K_TK_D^2$) down to pH 2, this trend at low pH would suggest that $K_T$ should continue to increase down to about pH 2.5 as shown by the dashed line in Figure 6. This enhances the difference between $K_D$ and $K_T$, further explaining why dimer populations were not observed at lower pH values. Moreover, if $K_{DT}$ increases at all above pH 5, the increase should originate from $K_T$ since, by eq 6, $K_D$ changes little, if at all, in the pH range from 5 to at least 7.

*Effect of Ionic Strength.* Since NaCl is used to dissociate PF4 from heparin–agarose and is naturally physiologically present, it may play a role in PF4 aggregation. Moreover, since PF4 aggregation is pH dependent, electrostatic interactions are probably involved in the association process, and varying the solution ionic strength can be used to explore this possibility. Figure 7 gives a series of NMR spectra at pH 4 and at a fixed PF4 concentration as a function of salt concentration. The initial conditions were chosen so that monomer, dimer, and tetramer species were present. On addition of 5 mM salt, it is apparent that the aggregation equilibrium is shifted in favor of the tetramer state. Estimation of $K_T$ and $K_D$ values as a function of NaCl concentration shows this more quantitatively in Figure 8. The magnitude of the equilibrium shift to the tetramer state varies with pH as shown in Figure 8 in terms of the overall equilibrium constant $K_{DT}$. The net effect of increasing ionic strength is more pronounced at lower pH values, consistent with the idea that intersubunit like-charge repulsion attenuates subunit association. At least at pH 4, $K_D$ seems more influenced by ionic strength than does $K_T$. Above 100 mM NaCl, monomer and dimer populations are too small to be accurately measured, and equilibrium constants could not be estimated.

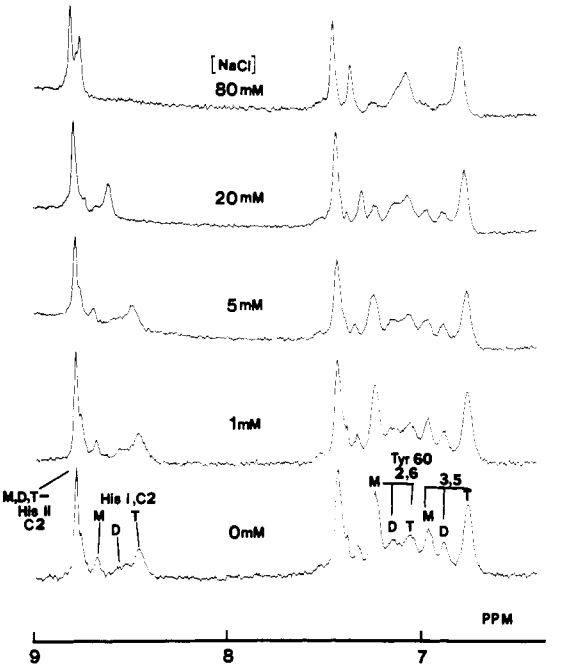


FIGURE 7: Effect of ionic strength. A series of NMR spectra for the aromatic proton resonance region of PF4 are shown as a function of the NaCl concentration as indicated in the figure. The protein concentration was 2 mg/mL at 303 K and pH 4.0 in $^2H_2O$.

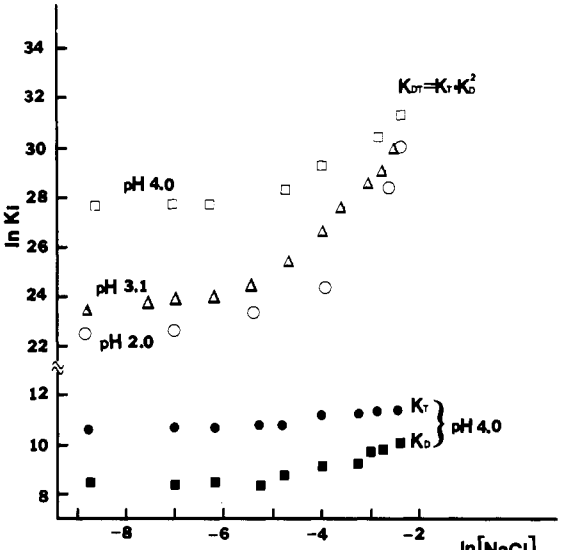


FIGURE 8: Effect of ionic strength on equilibrium constants. The natural logarithm of $K_T$ and $K_D$ at pH 4, and of $K_{DT}$ ($=K_TK_D^2$) at pH 2, 3.1, and 4, is plotted versus the natural logarithm of the NaCl concentration. The protein concentration was 2 mg/mL at 303 K, and the pH values are indicated in the figure.

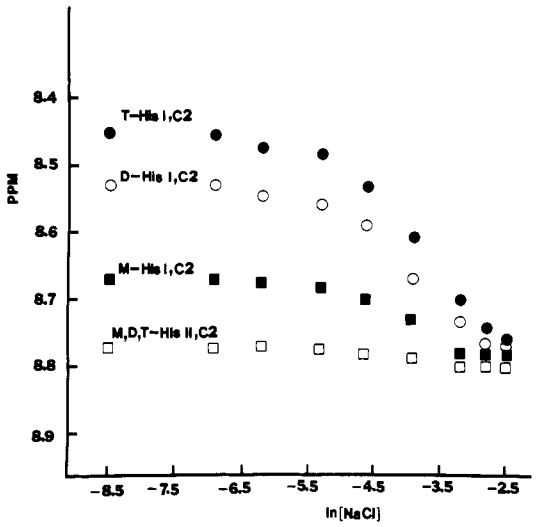


FIGURE 9: Chemical shifts of histidine versus NaCl concentration. The chemical shifts of His-I and His-II C2 proton resonances are plotted versus NaCl concentration at pH 4.0, 303 K. The resonance label prefixes M, D, and T stand for monomer, dimer, and tetramer states, respectively.

The Tyr-60 resonance chemical shifts are independent of salt concentration as they were for pH. The histidine-I resonances, however, are highly dependent on salt concentration, while His-II resonances are only slightly if at all dependent. Figure 9 plots the chemical shift of His C2 ring proton resonances versus the natural log of salt concentration. Up to about 2 mM, NaCl has little effect. By about 60–80 mM, the effect seems to have plateaued with an $IC_{50}$ value of about 20 mM. This value is apparently independent of pH. As a function of ionic strength, histidine chemical shift changes correlate to changes in equilibrium constants (Figure 8) and, therefore, are dependent on the state of aggregation. These shifts are probably mostly due to differences in histidine $pK_a$ values which vary with the state of aggregation as discussed in the next section. At lower pH values, these chemical shift variances are attenuated.

*Effect of Aggregation on Aromatic Side Chains.* As judged by NMR data, aggregation has little if any apparent effect on His-II while it has a significant effect on His-I and Tyr-60. Figure 10 plots the chemical shift of monomer, dimer, and tetramer histidine-I and -II C2 proton resonances versus pH. The His C2 proton resonances were assigned to each state at a given pH value only after careful analysis of extensive concentration and pH dependence data some of which are shown, for example, in Figure 4. His C4 proton resonances were generally not as well resolved and have not been considered here. His-II C2 proton resonances also can be bearly resolved for monomer and tetramer/dimer species. A His-II monomer $pK_a$ value of 5.9 can be estimated by using the Henderson–Hasselbalch equation (Lehninger, 1978) and by assuming an overall chemical shift change of 1 ppm between fully protonated and fully unprotonated states. The His-II tetramer/dimer $pK_a$ value is around 5.8. His-I C2 proton resonances are considerably more shifted than those of His-II and allow $pK_a$ estimates of 4.7, 4.3, and 4.2 for monomer, dimer, and tetramer species, respectively. In both the His-I and His-II cases, resonance broadening near $pK_a$ values (Figure 4) is most probably due to exchange between acidic and basic forms of histidine (Patel et al., 1972).

Monomer Tyr-60 ring proton resonances are upfield shifted by about 0.07 ppm on going to the dimer state and by about 0.2 ppm on going to the tetramer state. These shifts are accompanied by line-width changes; monomer Tyr-60 ring

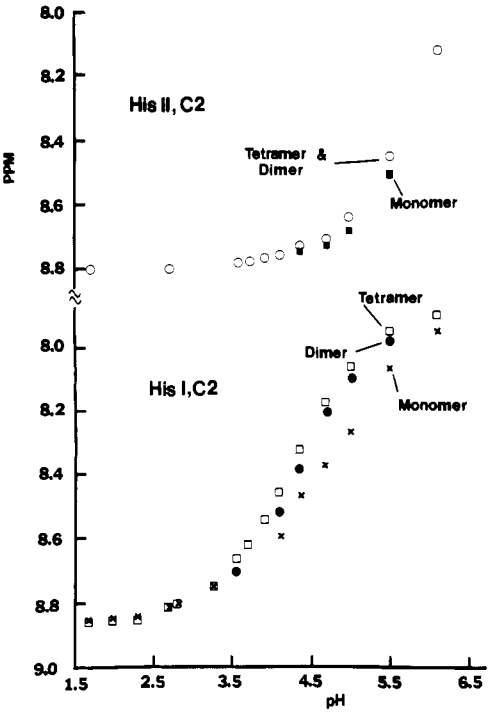


FIGURE 10: pH effect on the histidine C2 proton resonance. The chemical shifts of the His-I and His-II C2 proton resonances are plotted versus pH. Monomer, dimer, and tetramer species display varying chemical shifts as indicated in the figure.

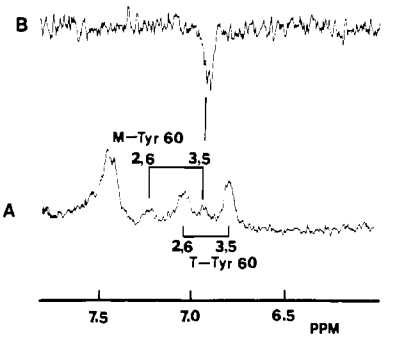


FIGURE 11: Photo-CIDNP difference spectrum. A 360-MHz proton NMR reference spectrum taken with a PF4 concentration of 2 mg/mL in 0.5 M NaCl/$^2H_2O$ solution at pH 3 and 298 K is shown at the bottom of the figure (A). Flavine dye (0.4 mM) was added to the sample for the photo-CIDNP experiment. The photo-CIDNP difference spectrum is shown at the top of the figure (B).

proton resonance line widths are about 20 Hz at half-height while they are increased to about 40 Hz in the tetramer state. Line-width increases are expected on aggregation, while chemical shift changes are difficult to interpret.

A photo-CIDNP proton NMR difference spectrum of PF4 is shown in Figure 11. The PF4 sample contained about 80% tetramer and 20% monomer under the conditions of this experiment. Photo-CIDNP spectroscopy can give one information on the relative "solvent" exposure of tyrosine, histidine, and tryptophan residues (Kaptein, 1978). Figure 11 shows that Tyr-60 is exposed to the flavine dye used to induce the photo-CIDNP response only in the monomer state. Although 4 times as many moles of Tyr-60 are present in the tetramer state, no apparent photo-CIDNP effect is observed at that resonance. This suggests that on aggregation, at least in the tetramer state, Tyr-60 becomes more internalized in the protein matrix. This could result either from an aggregation-induced conformational change in the monomer subunits or from involvement of Tyr-60 in the intersubunit binding domain(s). Neither histidine gives a photo-CIDNP effect; generally,

histidine gives a relatively small effect which could be diminished due to its protonation state (Kaptein, 1978).

## Discussion

That PF4 forms tetramers in solution has been known for some time (Moore et al., 1975). This present NMR study has yielded information on the mode or sequence of association, the relative strength of monomer subunit associations, and the nature of the interactions themselves. Resonance assignments have been made for Tyr-60, His-I, and His-II in monomer, dimer, and tetramer states under a variety of solution conditions. This has allowed us to easily monitor PF4 aggregation. These data show that the first step in PF4 association is dimer formation. Under most solvent conditions, the dimer population is minimal, and dimers readily associate to form tetramers. pH and ionic strength significantly influence dimer and tetramer association reactions, suggesting that electrostatic forces are intricately involved in the process. As the pH is decreased from about 5, both the dimer and tetramer dissociation reactions are enhanced. The dimer–dimer association reaction reaches a minimum at approximately pH 4; below this point, the tendency for dimer–dimer association rises with decreasing pH. The monomer–monomer association reaction, on the other hand, is continually attenuated down to pH 2.

X-ray structure analysis of the tetramer of the 14–85-residue fragment of bovine PF4 (St. Charles et al., 1989) shows that the crystal arrangement of the four monomer subunits (identified as A, B, C, and D) is such that two types of dimers are identified, i.e., AB(CD) type and AC(BD) type. This quaternary, structural arrangement may be conserved in tetramer human PF4 in solution. The present NMR data indicate the presence of one apparent dimer resonance reflected in the Tyr-60 and His-I populations, suggesting that one of these two possible dimers is more thermodynamically favored in solution. It is possible, however, that both AB- and AC-type dimers do form, with their respective ring proton resonances overlapping. The proposal for dimer preference is supported, moreover, by the observation of two different pH trends, one for monomer–monomer association ($K_D$) and one for dimer–dimer association ($K_T$). If no preference existed, then the effect of pH would have been the same, an average of both types. In AC-type dimers of bovine PF4, two salt bridges have been proposed between Glu-43 in one subunit and Lys-65 in the other subunit. No salt bridges were proposed in AB-type dimers. Assuming structural analogy to human PF4, this would suggest the presence of intersubunit salt bridges between Glu-28 and Lys-50. Tentative identity of the favored solution dimer as the AC type can be made by considering p$K_a$ values of interacting charge groups derived from monomer–monomer ($K_D$) association equilibrium data (Figure 6; eq 8). The best fit of eq 8 to these data yielded dimer-state p$K_a$ values of 2.3 and 10.3 for the two interacting groups. The existence of a salt bridge between Glu and Lys residues in PF4 AC-type dimers is consistent with these p$K_a$ values.

Electrostatic interactions involved in dimer–dimer (tetramer) association seem more complex and cannot be explained simply by two interacting oppositely charged residues. The decrease in $K_T$ as the pH is lowered to about 4.2 is probably the result of side chain protonation perhaps of carboxylate or histidyl groups. The enhancement of dimer–dimer associaton as the pH is further lowered is less clear, but may be due to protonation of proximal carboxylate groups on opposing subunits which could enhance certain hydrophobic interactions and/or protonation of a histidine residue with a resulting favorable anionic side chain interaction on an opposing subunit. The His-I p$K_a$ is 4.2 in the tetramer state. Interestingly, both explanations are possible for AB-type dimers in bovine PF4 (St. Charles et al., 1989). There, Glu-43 in subunit A is directly opposite Glu-43 in subunit B via an antiparallel $\beta$-sheet structure. Moreover, Glu-43 is sequentially flanked on both sides by hydrophobic residues. Second, His-50 in subunit A is proximal to Asp-84 and the C-terminus carboxylate in subunit B. This would tend to strengthen the previous identity of AC-type dimers as the thermodynamically preferred dimer in solution. The AB-type dimer interaction would be equated with our dimer–dimer (tetramer) association. Since about 25% of the bovine PF4 structure remains unknown due to cleavage of the first 13 N-terminal residues and to crystal disorder of residues 14–23 (St. Charles et al., 1989), little more can be inferred at this time.

Increasing the ionic strength up to 0.1 M NaCl, as was done here, should, if anything, disrupt protein–protein associations if only favorable electrostatic salt bridge like interactions were involved in the association process. Our data show that PF4 subunit interactions, at least at relatively low pH values, are enhanced by addition of up to 0.1 M NaCl. This suggests that other forces are also intimately involved in the association process. These forces may arise from favorable hydrophobic interactions or unfavorable like-charge repulsive interactions as exist, for example, between the two glutamate residues in AB-type dimers. Long-range repulsive interactions are another viable force. Ionic strength increases would then attenuate such unfavorable charge interactions, while enhancing hydrophobic-type interactions. A consequence of the neglect of long-range electrostatic interactions in using eq 8 is essentially the assumption that no contribution to $\Delta\nu_H$ is made by other charged groups on the protein which are not directly influenced by or involved in the association reactions. Their proton binding energies, however, should be affected by association, with a resulting contribution to $\Delta\nu_H$ over the narrow pH range studied. Our estimated p$K_a$ values would, therefore, also be affected. On addition of 0.1 M NaCl, $K_D$ is increased by about a factor of 10 at pH 4, while $K_T$ is less affected. At pH 5, the effect of increasing ionic strength is minimal. By using eq 8, it can be approximated that only p$K_{1,M}$ and p$K_{1,D}$ would be appreciably changed to 4.7 and 3.0, respectively. This would in no way affect the proposal of a Glu–Lys salt bridge as discussed earlier.

Photo-CIDNP NMR experiments reveal that Tyr-60 is accessible to the flavine dye used to induce the CIDNP effect in the monomer state, but not in the tetramer state. This suggests that the association process either (1) induces a monomer subunit conformational change or dampens backbone flexibility/motions at or near Tyr-60 to effectively mask it from the solvent, or (2) buries Tyr-60 within the intersubunit domain(s). Some evidence from CD exists which suggests that PF4 monomer subunits possess slightly more helix structure when in the tetramer state (Villaneuva et al., 1988). Structural evidence on bovine PF4 tetramers (St. Charles et al., 1989) shows that the only major helical domain, i.e., Tyr-60 to the end of the C-terminus in human PF4, faces the hydrophobic $\beta$-sheet domain and sandwiches Tyr between it and the C-terminal helix. This C-terminal region is not directly involved in intersubunit binding domains. The former explanation for the photo-CIDNP results, therefore, is the more likely one.

Present evidence suggests that His-II and perhaps its immediate surroundings are neither involved in nor significantly affected by the association process. Three pieces of data seem to support this: (1) the His-II p$K_a$ of 5.8 is about that expected for a solvent-exposed histidine; (2) dimerization/tetramerization does not appreciably change the chemical shift or p$K_a$

Table I: Gibbs Free Energy of Association at 303 K

| | $\Delta G_I$ (kcal/mol) | | | |
|---|---|---|---|---|
| | pH 3[a] | pH 4[a] | pH 5[a] | bovine PF4[b] |
| monomer–dimer ($\Delta G_D$) | −3.6 | −5.4 | −6.6 | −10 |
| dimer–tetramer ($\Delta G_T$) | −8.1 | −6.6 | −8.4 | −18 |
| monomer–tetramer ($\Delta G_{total} = 2\Delta G_D + \Delta G_T$) | −15.3 (−19.5)[c] | −17.4 (−20)[c] | −21.6 | −38 |

[a] Values given in kilocalories per mole as calculated from eq 7. [b] $\Delta G$ Calculated on the assumption that in human PF4 2 salt bridges form from monomer association and 12 H bonds form from dimer assocation. Other contributions to $\Delta G_I$ were not included. [c] Estimated in the presence of 100 mM NaCl.

of His-II; and (3) the His-II line shape is apparently unperturbed by monomer interactions. While these reasons are not conclusive in themselves, comparison with His-I renders further support. Two observations of the behavior of His-I can be correlated with the association process: (1) His-I p$K_a$ values and chemical shifts are different in monomer, dimer, and tetramer states; and (2) the half-height line widths of His-I ring proton resonances are greater than those of His-II even at pH values far removed from its p$K_a$. Moreover, the His-I p$K_a$ value drops from 4.8 in monomer PF4 to 4.3 in dimer PF4 and 4.2 in tetramer PF4. The reduced p$K_a$ even in monomer PF4 may suggest inclusion in the protein matrix or proximity of His-I to an anionic side chain (Aune & Timasheff, 1971). The exact reason(s) for this is (are) still unclear. In bovine PF4, His-50 is partially buried in the protein matrix, while His-38 is part of an "external loop" (St. Charles et al., 1989). By analogy, in human PF4, His-II may be tentatively assigned to His-23 and His-I to His-35. His-50 in subunit A of tetramer bovine PF4 (His-35 in human PF4) is proximal to and becomes more masked by the final three C-terminal residues of subunit B (AB dimer interaction). No interaction is apparent between the His-38 (His-23 in human PF4) domain and any other subunit.

Having learned something about the mode of subunit associations, their relative strengths, and the nature of their interactions, it is interesting to evaluate association energetics and compare them to possible structural interactions by analogy to bovine PF4. The Gibbs free energy, $\Delta G_I$, of protein–protein association can be estimated from these equilibrium constants, $K_I$, by using eq 9 where $R$ is the gas constant

$$\Delta G_I = -RT \ln K_I \quad (9)$$

[1.98 cal/(mol·K)] and $T$ is the temperature in Kelvin ($T$ = 303 K in these studies). These $\Delta G_I$ values are given in Table I for monomer to dimer, $\Delta G_D$, and dimer to tetramer, $\Delta G_T$, associations at pH 3, 4, and 5. $\Delta G_{total} = 2\Delta G_D + \Delta G_T$ is also given. It must be noted that these free energies have been derived from a single temperature measurement; as such, they are merely first-approximation estimates. The Gibbs free energies are the sum total of all favorable and unfavorable forces in PF4 subunit interactions. If we assume that human PF4 associates in a similar manner as does bovine PF4 (St. Charles et al., 1989), then we can sum up the more dominant forces of association, i.e., H bonds and salt bridges. These values are also given in Table I. The AC dimer which we have equated with $\Delta G_D$ is stabilized by the formation of two Glu/Lys salt bridges. Each salt bridge contributes about 5 kcal/mol to $\Delta G_D$ (Ghelis & Yon, 1982). Each AB dimer which we have equated with $\Delta G_T$ is stabilized by the formation of six antiparallel $\beta$-sheet H bonds. Each H bond contributes about 1.5 kcal/mol to $\Delta G_T$ (Ghelis & Yon, 1982). Not included in these estimates (Table I) are various hydrophobic interactions which lower the $\Delta G_I$ value and repulsive, like-charge interactions which raise the $\Delta G_I$ value. In particular, the AB dimer contains two adjacent, $\beta$-sheet interchain Glu residues which surely increase the $\Delta G_T$ value given in Table I. Considering the experimentally derived $\Delta G$ values, as the pH is raised to about 7 and the ionic strength is increased to attenuate long-range repulsive interactions, $\Delta G_D$ and $\Delta G_T$ should both decrease. With that trend in mind, the magnitudes of actual ($K_{eq}$ derived) and calculated (bovine PF4 analogy) $\Delta G_I$ values approach the same range. These estimates from bovine PF4 depend on many factors not discussed and are given only as a crude range. The forces which stabilize bovine PF4 subunits, therefore, probably also stabilized human PF4 subunit associations.

## Acknowledgments

We thank Prof. R. Kaptein for the use of his photo-CIDNP NMR spectrometer and Dr. Klaas Dykstra for running the photo-CIDNP spectrum of PF4.

**Registry No.** PF4, 37270-94-3.

## References

Aune, K. C., & Timasheff, S. N. (1971) *Biochemistry 10*, 1609–1617.

Aune, K. C., Goldsmith, L. C., & Timasheff, S. N. (1971) *Biochemistry 10*, 1617–1625.

Barber, A. J., Kaser-Glanzmann, R., Jakabova, M., & Luscher, E. F. (1972) *Biochim. Biophys. Acta 286*, 312–329.

Brindley, L. L., Sweet, J. M., & Goetzl, E. J. (1983) *J. Clin. Invest. 72*, 1218–1223.

Busch, C., & Owen, W. G. (1982) *J. Clin. Invest. 69*, 726–729.

Busch, C., Dawes, J., Pepper, D. W., & Wasteson, A. (1980) *Thromb. Res. 19*, 129–138.

Capitanio, A. M., Niewiarowski, S., Rucinski, B., Tuszynski, G. P., Cierniewski, C. S., Hershock, D., & Kornecki, E. (1985) *Biochim. Biophys. Acta 839*, 161–173.

Cowan, S., Bakshi, E. N., Machin, K. J., & Isaccs, N. W. (1986) *Biochem. J. 234*, 485–488.

Deuel, T. F., Kein, P. S., Farmer, M., & Heinrikson, R. L. (1977) *Proc. Natl. Acad. Sci. U.S.A. 74*, 2256–2258.

Deuel, T. F., Senior, R. M., Chuang, D., Griffin, G. L., & Heinrikson, R. L. (1981) *Proc. Natl. Acad. Sci. U.S.A. 78*, 4584–4587.

Ghelis, C., & Yon, J. (1982) *Protein Folding*, pp 136–176, Academic Press, New York.

Hermodson, M., Schmer, G., & Kurachi, K. (1977) *J. Biol. Chem. 252*, 6276–6279.

Holt, J. C., & Niewiarowski, S. (1985) *Semin. Hematol. 22*, 151–163.

Jeener, J., Meier, B., Backman, P., & Ernst, R. R. (1979) *J. Chem. Phys. 71*, 4546–4550.

Kaptein, R. (1978) in *NMR Spectroscopy in Molecular Biology* (Pullman, B., Ed.) pp 211–229, Reidel, Amsterdam.

Katz, I. R., Thorbecke, G. J., Bell, M. K., Yim, J. Z., Clarke, D., & Zucker, M. B. (1986) *Proc. Natl. Acad. Sci. U.S.A. 83*, 3491–3495.

Laterra, J., Norton, E. K., Izzard, C. S., & Culp, L. A. (1983) *Exp. Cell Res. 146*, 15–27.

Lehninger, A. L. (1978) *Biochemistry*, Worth Publishers, New York.

Lowry, O. H., Rosbough, N. J., Fan, A. L., & Randall, R. J. (1951) *J. Biol. Chem. 193*, 265–270.

Marcum, J. A., McKenney, J. B., & Rosenberg, R. D. (1984) *J. Clin. Invest. 74*, 341-350.
Marion, D., & Wüthrich, K. (1984) *Biochem. Biophys. Res. Commun. 113*, 967-974.
Mayo, K. H., Holt, J., Rucinski, B., & Niewiarowski, S. (1989) *J. Mol. Biol.* (submitted for publication).
Moore, S., Pepper, D. S., & Cash, J. D. (1975) *Biochim. Biophys. Acta 379*, 379-384.
Patel, D. J., Woodward, C. K., & Bovey, F. A. (1972) *Proc. Natl. Acad. Sci. U.S.A. 69*, 599-602.
Perlmann, G. E., & Longsworth, L. G. (1948) *J. Am. Chem. Soc. 70*, 2719-2724.
Rucinski, B. S., Stewart, G. J., Defeo, P. A., Bodeu, G., & Niewiarowski, S. (1987) *Proc. Soc. Exp. Biol. Med. 186*, 361-367.
Rucinski, B. S., Niewiarowski, S., James, P., Walz, D. A., & Budzynski, A. Z. (1979) *Blood 53*, 47-62.
Senior, R. M., Griffin, G. L., Huang, J. S., Walz, D. A., & Deuel, T. F. (1983) *J. Cell Biol. 96*, 382-385.
St. Charles, R., Walz, D. A., & Edwards, B. F. P. (1989) *J. Biol. Chem. 264*, 2092-2099.
Tanford, C. (1961) *Physical Chemistry of Macromolecules*, pp 286-296 Wiley, New York.
Villaneura, G. B., Allen, N., & Walz, D. A. (1988) *Arch. Biochem. Biophys. 261*, 170-174.
Waddell, W. J. (1956) *J. Lab. Clin. Med. 48*, 311-314.
Walz, D. A., Wu, V. Y., de Lamo, R., Dene, H., & McCoy, L. E. (1977) *Thromb. Res. 11*, 893-898.
Wyman, J. (1964) *Adv. Protein Chem. 19*, 224-250.

# Structural and Dynamic Differences between Normal and Transforming N-ras Gene Products: A $^{31}P$ and Isotope-Edited $^{1}H$ NMR Study†

Sharon Campbell-Burk‡
*Department of Biochemistry, Brandeis University, Waltham, Massachusetts 02254*
*Received March 29, 1989; Revised Manuscript Received July 21, 1989*

ABSTRACT: [$^{15}N$]Glycine was biosynthetically incorporated into normal cellular N-ras p21 and a position 12 transforming mutant, in order to produce p21 proteins containing several site-specific NMR probes at or near activating positions in the guanine nucleotide binding domain. We have previously assigned all five glycine resonances located in loops directly involved in binding of guanosine diphosphate in the wild-type p21 protein [Campbell-Burk, S., Papastavros, M. Z., McCormick, F., & Redfield, A. G. (1989) *Proc. Natl. Acad. Sci. U.S.A 86*, 817-820]. In this report, the corresponding glycine resonances in the p21 mutant have been assigned, and spectral differences between normal and mutant p21-guanosine diphosphate (p21·GDP) complexes have been investigated. Our combined $^{1}H\{^{15}N\}$ and $^{31}P$ NMR results show that substitution of aspartate for glycine-12 produces perturbations in the phosphoryl binding domain, near the point of the mutation. Although many of the remaining glycines were unaffected, spectral differences were also observed outside the GDP binding domain. Two of the five active-site glycines in wild-type p21·GDP have very slow amide proton exchange rates with water ($k < 2.8 \times 10^{-5}$ s$^{-1}$). The active-site glycines are located in solvent-exposed loops, so their apparent solvent inaccessibility may result from strong hydrogen bond formation between glycine amide protons and bound guanine diphosphate and/or other nearby groups in p21.

The most prevalent oncogene found in human cancer belongs to the ras gene family (Nishimura et al., 1987). There are three well-characterized classes of mammalian ras genes (N-ras, K-ras, and H-ras) which encode highly related 21-kDa proteins [for a recent review, see Barbacid (1987)]. p21 proteins are located on the inner surface of the plasma membrane (Willingham et al., 1980; Furth et al., 1983), bind guanine nucleotides with high affinity (Scolnick et al., 1978; Papageorge et al., 1982; Finkel et al., 1984), and possess guanosinetriphosphatase (GTPase) activity (McGrath et al., 1984; Sweet et al., 1984; Gibbs et al., 1984; Manne et al., 1985).

Certain point mutations in the coding sequences of ras genes give rise to p21 proteins capable of inducing transformation-specific phenotypes. Mutant p21 proteins derived from cellular (N-ras) and retroviral (v-H-ras, v-K-ras) ras oncogenes have one to two amino acid substitutions at positions 12, 13, 59, and 61 (Tabin et al., 1982; Reddy et al., 1982; Taparowsky et al., 1982; Yuasa et al., 1983; Bos et al., 1985). These mutant proteins were found to possess lower guanosinetriphosphatase activity relative to their normal cellular homologues (Yuasa et al., 1983; Capon et al., 1983; Reddy et al., 1982). A large number of mutants were produced by site-directed mutagenesis, and their biochemical properties and transformation capabilities were characterized. A correlation was found between mutant proteins capable of stabilizing the GTP-bound conformation and loss in cellular growth control, suggesting that p21·GTP is the biologically active form.

Although the function of p21 proteins is currently unknown despite intensive investigation, similarities between p21 proteins and mammalian G-proteins have led to the hypothesis that p21 proteins may be involved in signal transduction (Halliday, 1984; Gilman, 1987). In analogy with the well-characterized adenylate cyclase regulating G-proteins, $G_s$ and $G_i$ (Gilman,

†This work was partially supported by USPHS Grants 5-F32-GM11847 and GM20168 to S.C.-B. and to A. G. Redfield and by the Cetus Corp.
‡Present address: E. I. du Pont de Nemours and Co., Inc., CR&D, Wilmington, DE 19880-0328.

0006-2960/89/0428-9478$01.50/0 © 1989 American Chemical Society